PHYSICAL REVIEW E **72**, 031303 (2005)

Pressure wave propagation in a granular bed

Stephen R. Hostler* and Christopher E. Brennen
California Institute of Technology, Pasadena, California 91125, USA

(Received 28 February 2005; revised manuscript received 13 July 2005; published 21 September 2005)

The transmission of pressure waves in granular materials is complicated by the heterogeneity and nonlinearity inherent in these systems. Such waves are propagated through particle contacts primarily along the "force chains" which carry most of the load in granular materials. These fragile and ephemeral chains coupled with irregular particle packing lead to the observed heterogeneity. Nonlinearity in these systems is largely the result of the force-deformation characteristic at particle contacts. Through experiments and simulations, we study the effects of heterogeneity and nonlinearity on the properties of pressure waves through a granular bed.

DOI: 10.1103/PhysRevE.72.031303 PACS number(s): 45.70.−n, 62.30.+d

I. INTRODUCTION

Wave propagation within a granular medium is a complicated process that is important not only in a broad range of technological and natural contexts but also because of the potential it has for the interrogation of the state of that medium. While there are circumstances in which the interstitial fluid plays an important role in the wave propagation (see, for example, the fluidized bed research of Gregor and Rumpf [1], Musmarra *et al.* [2], and Weir [3] or the shock waves of Ben-Dor *et al.* [4]) we choose to focus here on the simpler circumstances of a relatively static bed in which the interstitial fluid plays a negligible role. Rather the wave propagation involves transmission through the particles and from particle to particle through the contact points. Experiments on wave propagation in beds of randomly arranged grains [5] and matrices of specific packings [6] revealed propagation speeds that, as expected, seemed to scale with the elastic wave speed in the material of the particles ($\sqrt{E/\rho}$ where E is the Young's modulus and ρ is the density) and showed little dependence on particle size. The speed did seem to increase somewhat with the overall constraining pressure or overburden pressure p. An assumption of Hertzian contacts between the particles [7,8] led Duffy and Mindlin [6] to theorize a speed that increased like $p^{1/6}$. The measurements follow this dependence at higher pressures but the behavior at lower confining pressures is more like $p^{1/4}$. Goddard put forward two possible explanations for this stronger dependence at lower pressures: first, that conical asperities may dominate the interaction between particles and, second, that the coordination number (the number of contacts) would increase as the pressure increased [9]. These could explain the $p^{1/4}$ dependence at lower pressures. Makse *et al.* [10] conducted simulations that supported the coordination number explanation; the simulations also yielded wave speeds in good agreement with the experimental measurements. We note that Velický and Caroli [11] proposed another explanation for the $p^{1/4}$ dependence that identifies disorder-induced stress fluctuations as responsible.

However, any review of the literature will clearly unveil a disturbingly broad range of measured values for the wave speed in granular beds particularly at lower pressures and it is difficult to correlate this range with the material properties involved. At low pressures the wave speeds range from 50 m/s [12] to 210 m/s [5] to 500 m/s [13] for glass or sand (see Ref. [14] for details). Stresses in a static granular bed are carried by "force chains," preferentially stressed chains of particles that are responsible for the nonisotropic distribution of stress in a granular material [15,16]. Stress waves are therefore propagated primarily along these force chains. The complication is that force chains can be altered as a result of very small perturbations. This heterogeneous and ephemeral nature of a granular bed is one possible explanation for the above-described discrepancies. It leads to complicated and often elusive wave propagation characteristics that are the subject of this paper.

Liu and Nagel investigated wave propagation in a bed of 5-mm glass beads using an accelerometer of a size comparable to an individual grain; thus they were detecting the wave transmitted through a single force chain. Though the waves seemed to be nondispersive in a general, average sense, the experiments yielded wave speeds that were highly susceptible to very small perturbations in the bed. This suggested an extreme fragility in the force chain microstructure; indeed the stress waves may themselves be altering that structure and therefore the local wave speed [17]. Jia *et al.* further addressed these issues and distinguished between propagation at low frequencies where the wavelength is long compared with the particle size and waves in several force chains will retain coherence. In contrast, waves at high frequency where the wavelength is comparable with the particle size will lack coherence at any detector [13]. Later we refer to this limit of Jia *et al.* which, according to their analysis, would occur around 50 kHz for 4-mm glass beads.

The purpose of this paper is to delve further into these intricate complications of wave propagation in a granular material, utilizing wave propagation measurements and simulations in beds of particles of different size and material. In addition to the wave propagation speed, we also examine the attenuation which is of considerable technological interest since granular materials are often used for acoustic insulation. There are several mechanisms by which wave energy is dissipated in a granular medium. Energy is clearly dissi-

---

*Currently at the Department of Mechanical and Aerospace Engineering, Case Western Reserve University. Electronic address: hostler@case.edu

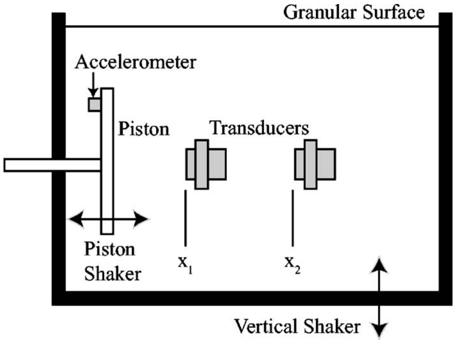

FIG. 1. Schematic of the experimental setup.

pated through frictional and inelastic particle interactions. In addition energy may be dissipated by irreversible particle rearrangement. Third, the wave energy may be scattered during propagation through the particle contact network. The literature contains few measurements or analyses of attenuation, perhaps because, as we shall see, the results are even more scattered than those for the speed.

II. EXPERIMENTS

The experiments (Fig. 1) utilized several clear, Plexiglas boxes (25×25 cm^2 or 84×25 cm^2 in planform) filled with granular material to a depth of 16.5 cm by pouring in particles while avoiding any unnecessary compaction of the bed. This procedure defined the loose state of the bed. A circular piston (diameter 10 cm, thickness 0.64 cm, center 8 cm above floor) driven by an electromechanical shaker was used to propagate wavelike disturbances horizontally across the box. The vibration frequencies ranged from Hz to kHz, and the amplitudes were monitored by an accelerometer attached to the back of the disk. Two strain-gauge pressure transducers with active faces 1.9 cm in width were buried in the bed at the same depth but at different distances from the piston. The near transducer is typically placed 50 mm from the piston, and the far transducer is located 50 mm or more beyond this point. They are held fixed from above with laboratory clamps and offset laterally so that the near transducer minimally obstructs the propagation of the signal to the far transducer. The clamping was needed to avoid transducer movement and had little effect on the transducer results. Finally, the entire apparatus was mounted atop a second electromechanical shaker which provides agitation of the bed through vertical shaking. This was used in the experiments for two purposes. To create a consolidated bed state, the bed was shaken for several minutes at a frequency of 20 Hz and an acceleration amplitude over $1g$. During this time, the height of the granular surface decreased by about 1 cm. The result was termed a consolidated state. A second use of shaking was to create an agitated state in which to make measurements and observations; the results of this investigation are reported in a separate paper.

Because of concerns about wave reflection from the box walls, the box was lined with foam. However, this had no discernable effect on the results since the wave attenuation was sufficiently high that almost all of the wave energy was dissipated before a wave could complete a reflection. In most cases, the foam was only used behind the piston between it and the box wall because that represented the shortest reflection path. Moreover, in this configuration, grains only contacted the front face of the piston and thus the piston was less constrained.

TABLE I. Material properties of the granular materials used in the experiments.

Material	Shape	$\rho(\mathrm{kg/m^3})$	E(GPa)	ν	c_0(m/s)
Glass	Spherical	2500	70.3	0.220	5300
PVC	Cylindrical	1500	2.75	0.420	1350

Measurements of the wave speed in the granular bed were made for both single input pulses and for continuous sinusoidal pulsing. In both the difference in the arrival time of the wave at the two transducers was used to determine a wave speed and the ratio of the measured wave amplitudes was used to determine an attenuation rate. In the single-pulse experiments, the wave arrival time was measured directly: this is done by identifying the time at which the pressure departed significantly from its static value. In the continuous, sinusoidal input experiments, the phase shift between the signals arriving at the two transducers was found by cross correlation. In the graphs which follow the attenuation is presented using values of ξ defined by

$$\xi=\frac{\ln\dfrac{\Delta p_2}{\Delta p_1}}{x_1-x_2}, \tag{1}$$

where Δp_1 and Δp_2 are the transducer output amplitudes measured at distances x_1 and x_2, from the piston.

A variety of granular materials were used in the experiments, and their properties are listed in Table I. The glass beads with diameters ranging from 0.3 to 5 mm allowed for the examination of particle size effects. The plastic particles permitted the evaluation of different material properties, as characterized by E and ρ, and the effect of particle geometry. In contrast to the uniform, spherical geometry of the glass beads, the PVC particles were cylindrical with dimensions of 1 mm $\times$ 3 mm. It seems likely that the angularity of their contacts would affect the packing and rearrangement characteristics.

III. SIMULATIONS

Computer simulations were also carried out using a soft-particle, discrete element method (DEM) similar to others used in granular flows [15]. The program tracks a specified number of discrete elements (particles), advancing each by integrating the equations of motion. At any instant in time, the entire state of each particle is known. The particles are soft in the sense that collisions between particles (and between particles and the walls) have a nonzero collision time. This is in contrast to hard-sphere models (see, for example, Ref. [18]) in which collisions are binary and instantaneous, with resulting velocities determined by a coefficient of restitution.

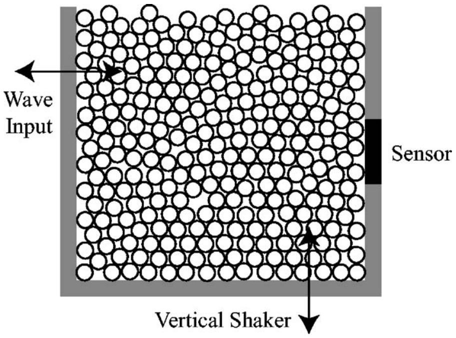

FIG. 2. Schematic of the simulation cell. Most of the simulations were conducted with a depth of about 77 particle diameters and a width of 50 particle diameters.

Soft-particle methods require a contact model to describe the forces throughout the collision process. The present simulations used a contact model comprised of the following.

(i) An elastic, Hertzian spring (force$=K_2\delta^{3/2}$) where δ is the particle overlap. Hertzian theory [8] gives $K_2 = 2ER_{eff}^{1/2}/3(1-\nu^2)$ where E is Young's modulus of elasticity, ν is Poisson's ratio, and $R_{eff}=R_1R_2/(R_1+R_2)$ is the effective radius of the colliding bodies of radii R_1 and R_2 (assumed composed of the same material).

(ii) A normal motion damper as in the model of Brilliantov *et al.* [19] such that the total outward normal force F_n is given by

$$F_n = \frac{2ER_{eff}^{1/2}}{3(1-\nu^2)}\delta^{3/2} + \frac{EAR_{eff}^{1/2}}{(1-\nu^2)}\delta^{1/2}\frac{d\delta}{dt}, \tag{2}$$

where the quantity A is related to material properties. Since the coefficient of restitution depends directly on this damping, the factor A was chosen to yield an appropriate coefficient of restitution.

(iii) A tangential spring similar to that used by Wassgren [20]. This tangential force increases linearly with a spring constant k_s until it reaches μF_n where μ is the coefficient of friction. Above this value it is set equal to μF_n. The tangential spring constant k_s was chosen to be one-tenth of a "normal spring constant" calculated by linearizing the Hertzian relation about a mean contact force given by the weight of material above that particular depth.

The time step interval was chosen to be one-tenth (or less) of the smaller of (1) the natural oscillation period of a particle and (2) the typical Hertzian contact time [7]. For further details the reader is referred to Ref. [14]. The above model is essentially quasistatic; we note the conditions listed by Nesterenko [21] for such a quasistatic model to apply—namely, (1) the material stresses in the particles should be less than the elastic limit, (2) the contact surfaces should be much smaller than the particles, and (3) the typical collision duration should be much larger than the natural oscillation period of particle distortions.

A schematic of the simulations is included as Fig. 2. They are two dimensional but use the masses and moments of inertia of spherical particles. Those reported herein used 4000 particles with some polydispersity in size (up to 10% in the diameter), a box width of 50 particle diameters, the above-mentioned ratio of tangential to normal spring constants, a value of $A^*=0.7$ (corresponding roughly to $\epsilon=0.8$ though ϵ will be velocity dependent), and a parameter $\rho g\bar{D}/E=1.74\times 10^{-9}$. The initial conformation of the bed is created by starting with the particles in a noncontacting array with random velocities and allowing the particles to sediment into a packed state.

Waves are created by moving the left wall, either in a sinusoidal or pulsed manner. For sinusoidal motion, the frequency and maximum displacement of the piston are specified. The single pulses (total width T_p) are triangular in velocity and consist of a period of constant positive acceleration followed by an equal period of negative acceleration of the same magnitude. Waves were detected in the bed with simulated pressure transducers in which the pressure is evaluated over some specified area of the container wall; any number of these sensors could be defined. After the initial settling phase of the simulations, the static pressure varies linearly with depth but only in an averaged sense. Even within one initialization of the bed, there is significant variation in the pressure at a particular depth and that scatter increases with depth. When considered in conjunction with the variation in stiffness implicit in Hertzian contacts this yields substantial point-to-point variation in the wave velocity.

IV. NONDIMENSIONALIZATION

Most of the results of both the experiments and the simulations are presented nondimensionally, and we consider here some dimensional analyses. The results presented were nondimensionalized using an average particle mass $\bar{m}$ (or density ρ), an average particle diameter $\bar{D}$, and an elastic wave speed within the particles, $c_0=\sqrt{E/\rho}$. The dimensionless normal force becomes $F_n^*=F_n\bar{D}/\bar{m}c_0^2$, the dimensionless overlap is $\delta^*=\delta/\bar{D}$, the dimensionless pressure per unit breadth is given by $p^*=p\bar{D}^2/\bar{m}c_0^2$, and the dimensionless time is $t^*=c_0t/\bar{D}$. It follows that in the contact model, K_2 and η are replaced by dimensionless quantities K_2^* and η^*, defined by

$$K_2^* = \frac{\bar{D}^{5/2}K_2}{\bar{m}c_0^2} = \frac{4}{\pi(1-\nu^2)}R_{eff}^{*1/2}, \tag{3}$$

$$\eta^* = \frac{\bar{D}^{3/2}\eta}{\bar{m}c_0} = \frac{6}{\pi(1-\nu^2)}R_{eff}^{*1/2}A^*, \tag{4}$$

where $A^*=c_0A/\bar{D}$ and R_{eff}^* is $1/2$ for a particle-particle collision and $1/4$ for a particle-wall collision. These dimensionless parameters are functions of only ν and the coefficient of restitution. The expression corresponding to Eq. (2) then becomes

$$F_n^* = \frac{4R_{eff}^{*1/2}}{\pi(1-\nu^2)}\delta^{*3/2} + \frac{6R_{eff}^{*1/2}A^*}{\pi(1-\nu^2)}\delta^{*1/2}\frac{d\delta^*}{dt^*}. \tag{5}$$

For reference purposes note that while $A^*=0$ clearly yields collisions that are fully elastic in the normal direction, a

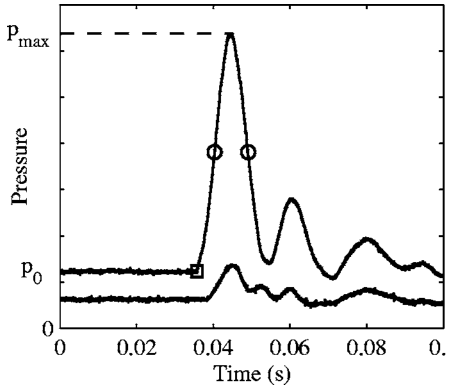

FIG. 3. Typical signals recorded by the two transducers as a result of a single input pulse. The point used to calculate the arrival of the wave is shown with a square. The width of the wave is determined at the location of the circles.

value of $A^*=10$ produces highly dissipative collisions with no appreciable rebound.

More generally, in an infinite domain of grains of size $\bar{D}$, Poisson's ratio ν and coefficient of restitution, ϵ, dimensional analysis yields a wave speed that must be proportional to $\sqrt{E/\rho}$ where the dimensionless factor of proportionality can only be a function of ν, ϵ, and the geometric configuration of the grains. Therefore, provided the deformations remain elastic, the acoustic speed will be independent of the particle size $\bar{D}$; in the absence of damping, the dimensionless acoustic speed will only be a function of ν and the configuration or packing of the grains.

The dimensionless damping $\xi\bar{D}$ should also be a function only of ϵ, ν, and the configuration. Then ξ should scale with $1/\bar{D}$; we return to this discussion the experimental results.

V. EXPERIMENTS WITH PULSED INPUT

The single-pulse experiments utilized simple compressive piston displacements that were unidirectional and returned to zero displacement at the end of the pulse. They are best characterized by the pressure pulse at the first transducer as exemplified by Fig. 3; the amplitude Δp is the difference between the maximum pressure p_{max} and the initial static pressure p_0; the pulse width is measured at one-half of that amplitude. Pulse widths varied between 1 ms and 100 ms, and amplitudes up to 3 kPa were examined. Wave propagation speeds were derived from the delay between first arrivals at the two transducers. First arrival was judged by a small, nonnoise departure from the ambient pressure p_0, as indicated in Fig. 3. The oscillations that follow the initial peak in Fig. 3 were typical, and more discussion of these is delayed until Sec. IX B.

The spatial decay of the pulsed wave is plotted in Fig. 4 for both glass and PVC particles. Clearly, the attenuation is substantially larger in the PVC with decay rates over twice that in the glass. However, all these attenuations are large in an absolute sense; for example, a pulse in the 3-mm glass was completely attenuated at a distance of 420 mm from the piston. The increased scatter at the smallest transducer spacing is a result of the comparably few particles that fill such a small space. Fewer particles lead to a small number of idiosyncratic wave paths.

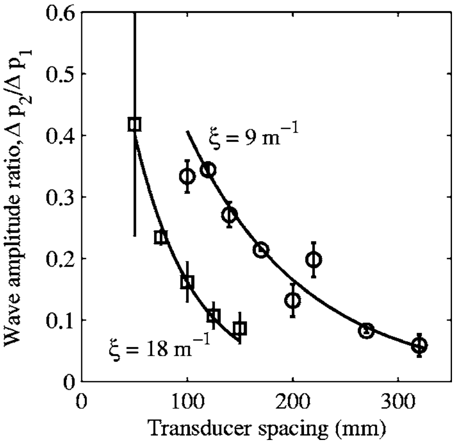

FIG. 4. Pressure amplitude ratio decay with increased distance between the transducers. The near transducer, with pressure amplitude Δp_1, is fixed at 50 mm from the piston while the far transducer is moved. Results for both 3-mm glass beads (○) and PVC cylinders (□) are shown. Each point is the mean of several points, and error bars show the standard deviation of the measurements. Also shown are lines corresponding to $\xi=9\ \mathrm{m}^{-1}$ and $18\ \mathrm{m}^{-1}$.

In one set of experiments, the input pulse amplitude was held fixed and the duration of the pulse (the input pulse width) was varied from 2 ms to 66 ms. At each setting of the width, four consecutive pulses were documented. If the bed were changing with time as a result of the pulses altering the force chains, the data would change between consecutive pulses. The effect of input pulse width on the shape of the detected pressure waves is illustrated in Fig. 5. For small input pulse widths, the wave consists of a single peak as in Fig. 3. The 4-ms and 14-ms pulses in the PVC and the 6-ms pulse in the glass beads are additional examples of such waves. This initial peak is followed by a series of oscillations around the static pressure value. As the input pulse width is increased, two changes are observed. First, the amplitude of the detected wave increases primarily because the dynamics of the piston drive allows more energy to be inserted during this longer pulse. More pertinent is the second effect—namely, the splitting of the individual peak into multiple peaks which is most evident between the 14-ms and 41-ms pulses. The largest input pulse width, 66 ms, shows that the additional peaks are oscillations, similar to those occurring about the static pressure value after the shorter single pulses have passed.

Figure 6 (top) presents the variation in the detected wave width with input pulse width and indicates two distinct regimes. For larger input pulse widths [greater than $T_p^*=1\times 10^4$ ($T_p=20$ ms)], the detected width scales with the input pulse width as one would expect. In this range, the wave width is always less than the pulse width, a result of measuring the wave width at the half-height. The more intriguing regime is at small input pulse widths [less than $T_p^*=5\times 10^3$ ($T_p=10$ ms)]. Here, the detected wave width is independent of the input pulse width. Regardless

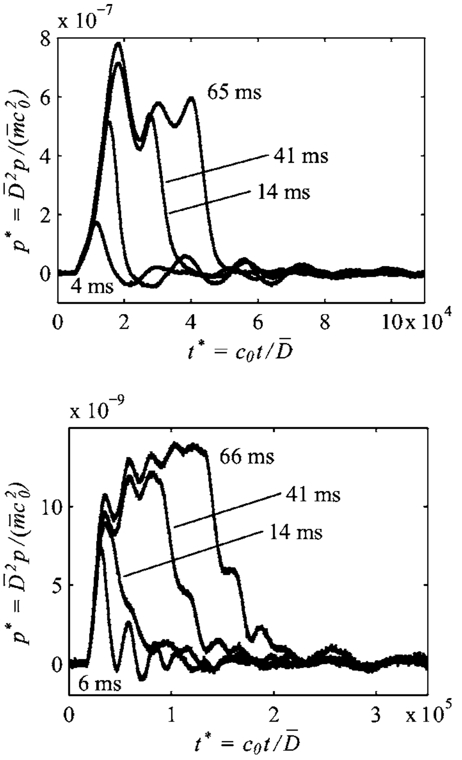

FIG. 5. Wave shapes at 50 mm from the piston for a fixed input pulse amplitude and four different input pulse widths. Top: PVC beads. Bottom: 3-mm glass beads.

of the input pulse width, the width of the detected wave is $T_w^*=5\times 10^3$ ($T_w=10$ ms). This corresponds to a disturbance with a frequency of roughly 50 Hz. Waves in this regime are "semipermanent" waves for which the input conditions have little effect on the wave shape (we use "semipermanent" rather than the conventional "permanent" because of the large attenuation). Semipermanent waves were also observed in simulations (see Sec. VI), where the wave width was nearly the same regardless of the shape or size of the pulse that created it. Further discussion on these semipermanent waves is delayed until Sec. IX A.

The bottom portion of Fig. 6 shows the ratio of the wave widths measured at the two transducers. Over most of the range of input pulse widths, wave broadening occurs. That is, the width measured at the far transducer is greater than that measured at the near transducer. Only the smallest input pulse widths show the opposite trend, and these points have a substantial uncertainty because of the weakness of the signals for these short pulse widths.

A second set of experiments was carried out to examine the effect of increasing the input pulse amplitude on the measured properties of the waves. The width of the input pulse was fixed and the pulse amplitude was varied.

Typical results in Fig. 7 (top) show the relationship between the voltage specified at the pulse generator and the pressure amplitude of the waves measured in the granular bed. For the smaller pulse amplitudes at the near transducer and at all pulse amplitudes for the far transducer, the measured wave amplitude increases in a regular monotonic manner as the input pulse amplitude is increased. However, for input pulse amplitudes greater than a critical value, the measurements at the near transducer begin to be scattered and the regular growth trend is broken with the wave amplitudes actually decreasing with increasing pulse amplitude. These behaviors are consistent with force chain rearrangement at the larger wave amplitudes. If one of the multiple force chains connecting the source and detector was broken, one would expect a drop in the measured pressure. Moreover, time-varying particle arrangements would account for the increased scatter. The fact that neither of these effects is seen at the far transducer further supports the hypothesis that particle rearrangement is occurring where the wave amplitude is large.

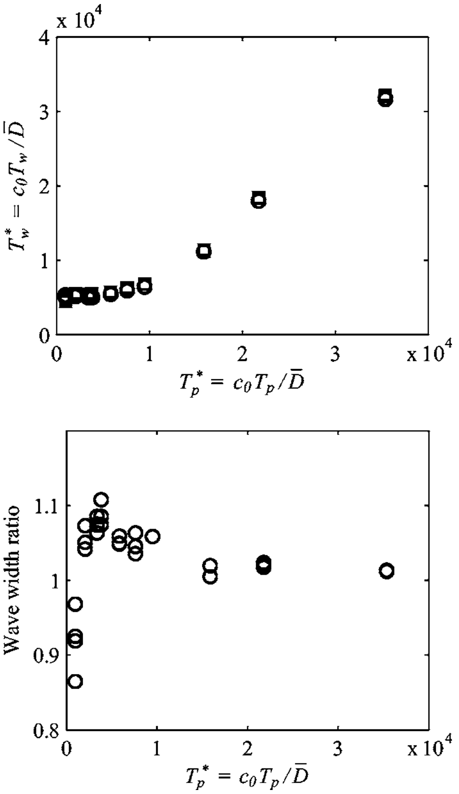

FIG. 6. Top: width of the detected pulse in PVC particles at transducers 50 mm (○) and 100 mm (□) from the piston as a function of the input pulse width. Bottom: the ratio of these pulse widths.

The width of the detected wave increases only modestly with increasing input pulse amplitude. This weak dependence is illustrated in Fig. 7 (bottom) which demonstrates that even within the semipermanent regime, the wave width still changes, albeit slightly, with the pulse amplitude. The scatter in the data increases at the largest pressure amplitudes.

The wave speeds measured in both the constant input amplitude and the constant pulse width experiments are presented in Fig. 8 where they are plotted against the amplitude of the wave detected at the near transducer. For all experiments, the measurements contain a substantial scatter that seems inevitable with ephemeral force chains and is particularly evident for the 3-mm glass particles. On average, the speed in the PVC particles is around 60 m/s; in the glass

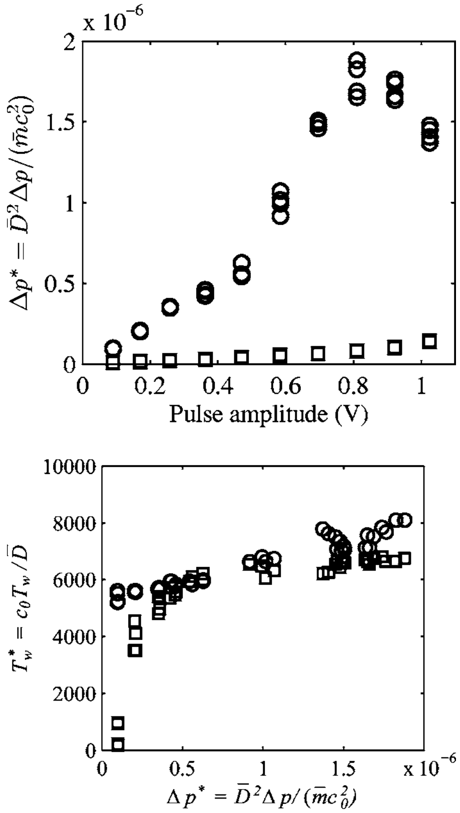

FIG. 7. Wave amplitude (top) and wave width (bottom) as functions of the input pulse amplitude for a fixed input pulse width of 6 ms. Measurements are made at transducers 50 mm (○) and 200 mm (□) from the piston in a bed of PVC cylinders.

beads the speed is higher, averaging about 120 m/s. Though the scatter is large, there is no clear indication of the wave speed changing with increasing wave amplitude.

One would expect consolidation of the granular bed to have a significant effect on its wave propagation characteristics. The denser state that results from consolidation leads to an effectively stiffer bed and reduces the possibility of rearrangement. Details of the consolidation procedure used in the present experiments can be found in Ref. [14].

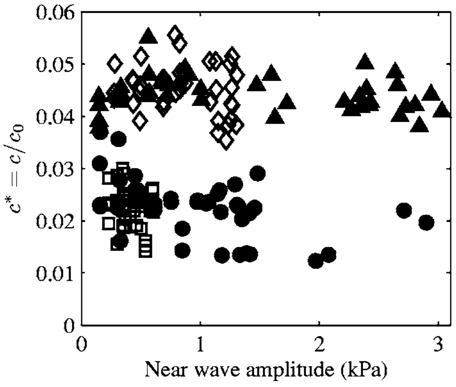

FIG. 8. Wave speed as a function of the wave amplitude measured at the near transducer. Both constant amplitude [PVC (◇), 3-mm glass (□)] and constant width [PVC (▲), 3-mm glass (●)] experiments are plotted.

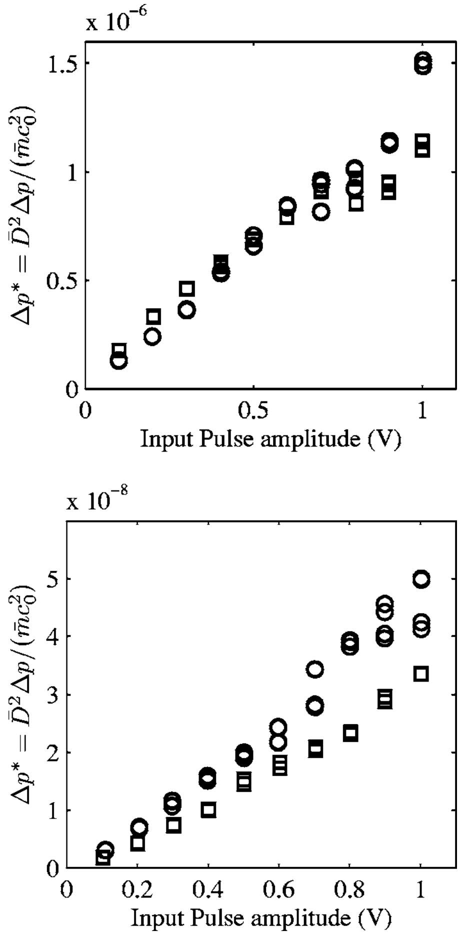

FIG. 9. Wave amplitude measured at 50 mm from the piston for an unconsolidated (○) and a consolidated (□) bed. Materials: PVC (top) and 2-mm glass spheres (bottom).

Figure 9 compares the measured wave amplitudes in consolidated and unconsolidated beds for both the PVC cylinders and 2-mm glass spheres. The same effects of bed rearrangement that were seen in Fig. 7 can be seen here. The regular increase in the wave amplitude with input pulse amplitude gives way at the larger pulse amplitudes to irregular, scattered data at the near transducer. In the glass particles, consolidation limits this effect. The linear increase in the wave amplitude continues past the point at which the data from the unconsolidated bed begins to diverge and scatter. It could be that the denser, consolidated bed impedes the piston motion and prevents magnitudes of the pressure disturbance for which rearrangement occurs. This cannot be the full explanation since the measured wave amplitude exceeds that at which the unconsolidated bed begins to scatter. It could also be that the consolidated bed is less fragile, so relative particle motion is less likely. The data from the bed of PVC particles show the same scatter regardless of consolidation. This may be a result of the relatively irregular shape of the PVC particles compared to the spheres. Force chains constructed from the cylinders may be less stable than those made from spheres.

The attenuations that correspond to the wave amplitude data in Fig. 9 are shown in Fig. 10. Consolidation consis-

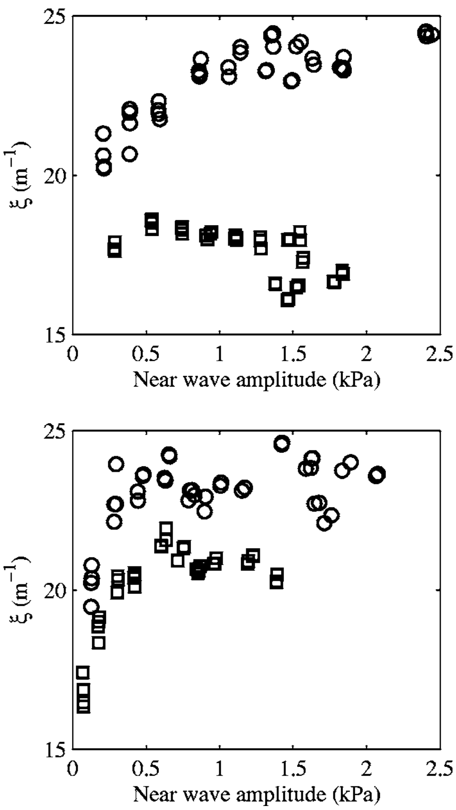

FIG. 10. Attenuation in an unconsolidated (○) and a consolidated (□) bed with increasing initial wave amplitude. Materials: PVC (top) and 2-mm glass spheres (bottom).

tently reduces attenuation in both materials and reduces the scatter in the data.

The results of wave speed measurements in both consolidated and unconsolidated beds for both PVC and glass are plotted in Fig. 11. For both materials consolidation noticeably increases the wave speed as expected.

VI. SIMULATIONS WITH PULSED INPUT

In this section, we examine the general characteristics of pulsed waves in the simulations and discuss the broad changes that occur with the change of parameters. Typical waves that result from a pulsed movement of the left wall of the simulation cell are shown in Fig. 12 and consist of a smooth positive pressure peak followed by a series of oscillations. This was found to be a general trend. As in the experiments, changes in the input pulse width over several orders of magnitude changed the detected transmitted wave width only slightly.

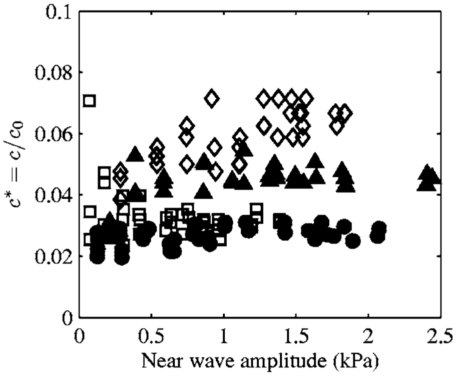

FIG. 11. Wave speed in beds of 2-mm glass and PVC particles. Results are shown for both the unconsolidated [glass (●), PVC (▲)] and consolidated [glass (□), PVC (◇)] states of each bed for increasing initial wave amplitude.

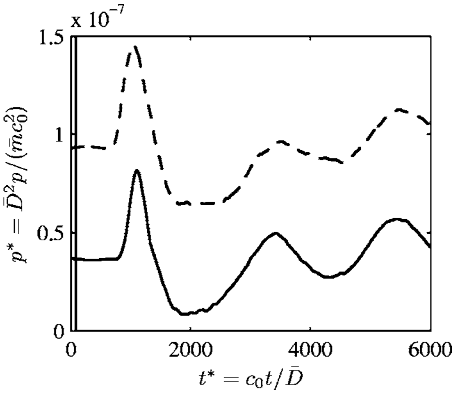

FIG. 12. Wave shape resulting from a pulsed movement of the left wall. Ratio of input displacement to static deformation is of order 10. Pressure is measured on sensors (10 particles high) on the right wall 50 particles (solid line) and 20 particles (dashed line) above the bottom with the bed free surface at 76 particles above the bottom. The pulse width is shown on the left of the plot.

Qualitative differences are seen in the wave structure as the amplitude of the input pulse is increased. Figure 13 shows the shape of the wave at the two detectors for an input pulse 10 times larger than that shown in Fig. 12. The wave is characterized by a comparatively steep leading edge that resembles a shock front. The trailing edge is less steep, but still tends to zero rather quickly with none of the oscillations that were observed for the smaller amplitude wave. This drop to zero pressure is a result of a much stronger reflection of the wave from the right wall. Zero pressure implies that the particles at the detector momentarily lose contact with the detector as they recoil from the wall. An enlarged view of the

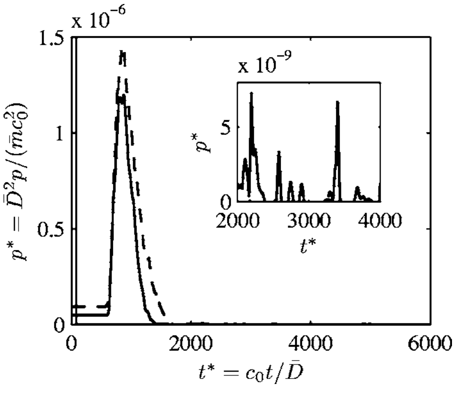

FIG. 13. Wave shape for a comparatively large amplitude pulse. Ratio of input displacement to static deformation on the order of 100. Pressure is measured on sensors (10 particles high) on the right wall 50 particles (solid line) and 20 particles (dashed line) from the bottom with a bed free surface at 76 particles. Inset is a detailed view of region behind the wave in which the pressure drops to zero.

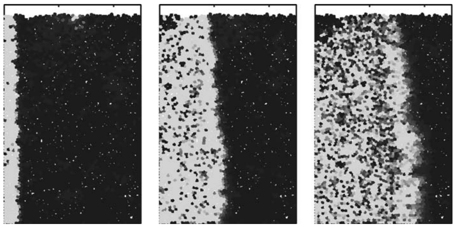

FIG. 14. Transmission of a pressure wave in a static granular bed. Frames taken at intervals of $t^{*}=250$.

zero-pressure region of the signal, as shown in the inset of Fig. 13, does reveal some collisional activity. The amplitude of these collisional peaks ($\Delta p^{*}\approx 4\times 10^{-9}$) is three orders of magnitude smaller than the wave amplitude, and the width of these peaks, in dimensionless time units, is in the range $t^{*}=50-70$. Such widths, as well as the shape of the pressure spike, are consistent with measurements made by Zenit [22] for the collision of a particle on the face of a high-frequency response pressure transducer.

Since the state of each particle is known entirely, an alternative way of visualizing the wave is to look at the instantaneous force between particles. Figure 14 is the result of such a visualization for the pulsed wave with a moderate pulse amplitude shown in the pressure traces of Fig. 12. Shading codes the magnitude of the net horizontal force on a given particle. Black corresponds to zero force, and white corresponds to a force value of $F_n^{*}=5\times 10^{-9}$. The effect of the pulsed motion of the left wall is seen in the first frame. The displacement of the wall creates a wave front that is parallel to the wall. As the wave propagates, the curvature of its front increases due to greater wave speed at greater depth. Another notable feature of the wave front is its irregularity which might be expected due to the heterogeneous nature of the bed. The size of the irregularities appears to grow with time. In the first frame, there are variations in the location of the front on the order of one particle diameter with some features deviating by as many as two particle diameters. By the third frame, irregularity elements are typically three particles diameters in size, but can be as large as six diameters.

The effect of dissipation is also seen as the wave evolves. The energy input into the bed is initially focused in a narrow band near the wall as denoted by the high concentration of white particles. By the third frame, this energy is spread over nearly the entire width of the bed, leading to a reduction in the magnitude of the forces between particles. The combination of this energy diffusion with energy lost to inelasticity in the particle contacts leads to a net dissipation of the energy of the coherent wave detected at the pressure sensor.

For times later than those depicted in the three frames of Fig. 14, some reflection of the wave from the right wall can be seen. After the first reflection, the wave becomes so weak and scattered that it can no longer be tracked as a coherent entity. Since no additional reflections can be observed, it is likely that the oscillations in the pressure traces are not due to reflections within the cell but to vibration of the force chains as has been hypothesized in the discussion of the experiments (see Fig. 21).

The computer simulations were also used to determine some of the specific functional dependences. Using a base line set given by $\nu=0.220$ and $A^{*}=0.7$ and a pulse with a displacement $d_{max}^{*}=4\times 10^{-4}$ and duration $T^{*}=80$, each of these four quantities was varied in turn to determine the functional consequences. First, the dependence of the wave speed on Poisson's ratio is shown in Fig. 15 (top). The speed increases only slightly with ν for typical values in common materials (the experiments had ν values in the range 0.22–0.42). The data in Fig. 15 (top) also show that the depth of the measurement in the bed has a significant effect on the wave speed. Depth increases the static pressure at which the wave speed measurement is made. The difference in the wave speed with depth is consistently greater than the scatter in the data. Figure 15 (bottom) shows the dependence of the wave speed on the displacement (amplitude) d_{max}^{*} of the input pulse. With increasing input pulse amplitude the wave speed increases by about 50% as d_{max}^{*} is increased from 1×10^{-4} (the smallest value for the waves could be accurately measured) to 1×10^{-2} (about 10% of the size of a particle). As might be anticipated, the wave speed c^{*} exhibits no significant dependence on the dissipation factor for expected A^{*} values between 0 and 1. Note also that the wave speed was only weakly dependent on the input pulse duration T_p^{*}, decreasing by about 20% as the duration was increased by two orders of magnitude from $T_p^{*}=8$ to $T_p^{*}=800$.

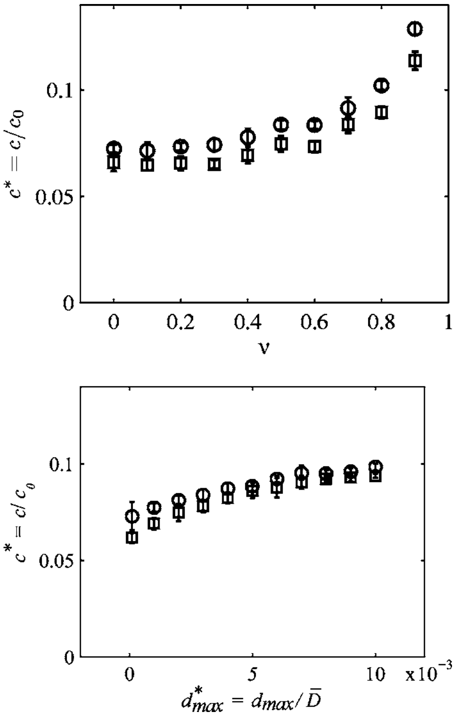

FIG. 15. Wave speed measured at detectors 20 (○) and 50 (□) diameters from the bottom of the cell for various values of Poisson's ratio (top) and of the maximum input pulse displacement, d_{max}^{*} (bottom). Five samples were taken for each ν value. The average of the resulting speeds is plotted with the standard deviation shown by error bars.

The variation of the wave amplitude with input pulse displacement, Fig. 16 (top), is similar to that observed in the experiments (see Fig. 7). At small displacements, the wave amplitude increases linearly with input pulse displacement. The slope is steeper for the measurement made deeper in the

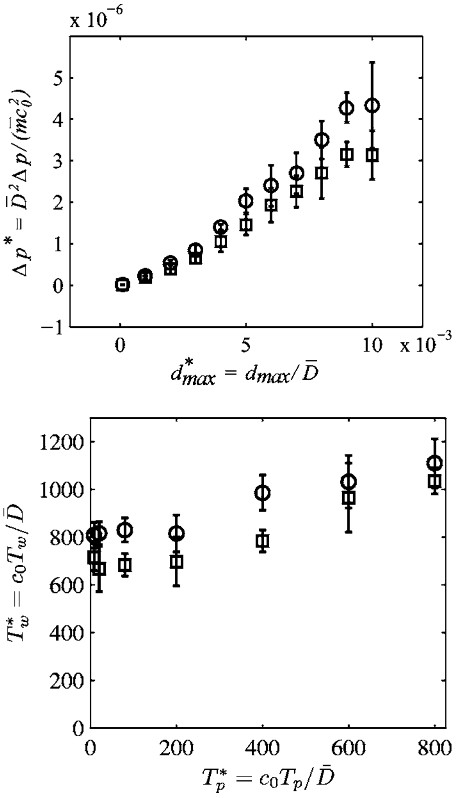

FIG. 16. Top: wave amplitude Δp^* for various values of the maximum input pulse displacement d^*_{max}. Bottom: wave width T^*_w for various values of the input pulse width T^*_p. Measurements at detectors 20 (○) and 50 (□) diameters from the bottom of the cell. Five samples were taken; the average is plotted with the standard deviation shown by error bars.

bed. The scatter in the data increases with increasing pulse amplitude. For the largest pulse displacements, the growth of the wave amplitude is no longer linear. The wave amplitude tends to level off at both detectors. In the experiments, the wave amplitude was seen to increase initially and then decrease unpredictably at large input pulse amplitudes. As in the experiments, these effects and the increased scatter with amplitude are due to bed rearrangement in the simulations.

The dependence of the wave width on the input pulse width is shown in Fig. 16 (bottom). At the lower input pulse widths, the wave width is constant and independent of the input pulse width whereas, above $T^*_p = 200$, the wave width increases linearly with the width of the input pulse. This is precisely the behavior observed in the experiments (Fig. 6) with the constant width at lower input widths being characterized as semipermanent waves.

VII. EXPERIMENTS WITH CONTINUOUS INPUT

We now shift attention to the experiments and simulations that employed continuous sinusoidal excitation. Two types of experiments were performed, the first by varying the excitation frequency while maintaining a constant piston acceleration amplitude. The intent is to establish the dispersion relation for the granular bed. Later, the results of performing experiments at a constant frequency while varying the amplitude will demonstrate the fragility of the bed and its susceptibility to force chain rearrangement as a result of disturbances as weak as the input pressure waves [17].

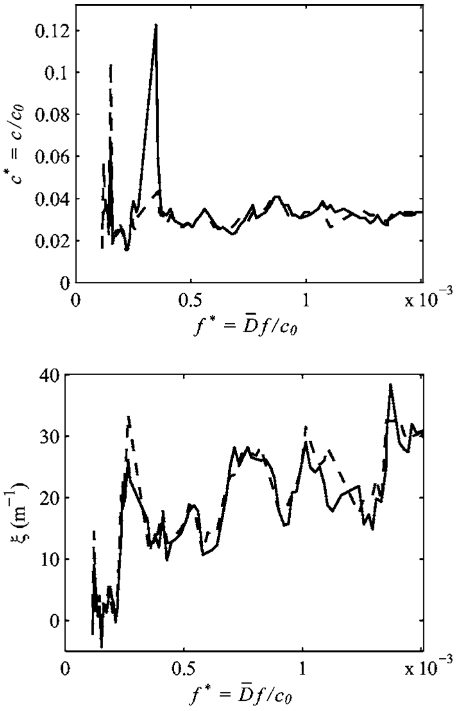

FIG. 17. Phase speed (top) and attenuation ξ (bottom) measured at constant acceleration values of $0.20g$ (solid line) and $0.30g$ (dashed line) in 4-mm glass beads at a spacing of 39 mm.

A. Constant-amplitude experiments

Figure 17 (top) is a typical result for the phase speed obtained from the constant-amplitude experiments by cross correlation of the transducer signals. In an overall way, the results tend to confirm the nondispersive character of wave propagation in a static granular bed as previously described by Liu and Nagel [23]. Measurements were made at two different input acceleration amplitudes, one immediately after the other at each frequency; hence particle rearrangement between the two amplitudes was minimized. This limited change in amplitude had little effect on the phase speed. However, Fig. 17 does show significant local departures from the mean propagation speed. The large departures at frequencies below about $f^* = 4 \times 10^{-4}$ ($f = 500$ Hz) could be attributed to resonant frequencies within the box (a half-wave in a 25 cm width with $c = 170$ m/s gives a resonance at 340 Hz) or to resonance frequencies of the piston assembly. The natural frequency of the piston and rod connecting it to the shaker was measured with an impact hammer and found to be 300 Hz. The natural frequency of the piston disk alone was measured as 400 Hz. But the significant variations in the wave speed at higher frequencies are inherent to these experiments. They occur between one experiment and the next under superficially identical conditions and are likely due to the specific and idiosyncratic contact stress distribution per-

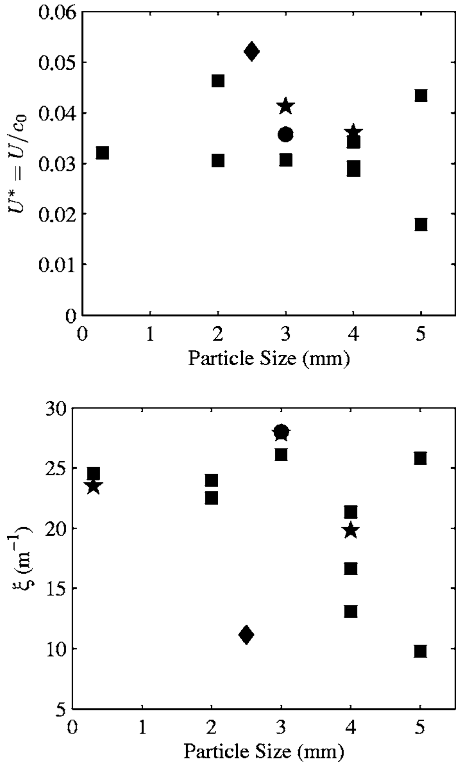

FIG. 18. Summary of the group velocity (top) and the attenuation (bottom) as functions of particle size. Data shown for PVC cylinders (♦) and glass spheres: unconsolidated (■), increased overburden (●), and consolidated (★).

taining in each experiment. As Liu and Nagel showed these distributions are fragile and ephemeral [17]. Averaging of multiple experiments causes these variations (and the dispersion they might imply) to disappear.

Evaluating the average phase speed at frequencies greater than $f^* = 4 \times 10^{-4}$ yielded the group velocities presented in Fig. 18 (top) for a variety of granular materials and experimental conditions. For the glass particles, the resulting group velocity is about $U^* = 0.03$ ($U = 170$ m/s) for nearly all particle diameters, bearing out the size independence of the wave velocity anticipated in Sec. IV. An exception is the point at $U^* = 0.046$ which can be attributed to a poor curve fit and the data points at the largest particle sizes where there is significant spread in the measurements. To measure the wave speed accurately, averaging must be done over multiple force chains. As the particle size increases relative to the fixed size of the transducer face, this averaging procedure begins to fail since few particles and few force chains are in contact with the transducer face. Specifically, the coherence of the averaging begins to break down for 4-mm particles and by 5 mm the accuracy of the measurement is severely reduced.

The strongest observed influence on the group velocity is the material composition of the particles, and the measurements in the PVC particles demonstrate this ($U = 65$ m/s). Scaling the group velocity in Fig. 18 (top) by $c_0 = \sqrt{E/\rho}$ partially accounts for the difference in material composition, but differences in ν between the two materials may be responsible for the remaining discrepancy in the values. The data in Fig. 18 (top) also show that consolidation and an increase in the overburden increase the group velocity as expected. The group velocities obtained in these continuous excitation experiments are comparable to those obtained in the single-pulse experiments (see Figs. 8 and 11). As long as the group velocity is measured on the coherent part [13] of the wave these measurements should correspond. Attenuation is so large in our system that the coherent portion of the wave is all that remains at the point of measurement.

The measurements of the attenuation ξ in Fig. 17 (bottom) display considerable irregularity. Even with small changes in the frequency, the attenuation varies by as much as a factor of 3. There is, however, a general increase in the attenuation with increasing frequency as might be expected. (Consolidation does not lead to any consistent trend in the attenuation.) Attenuations averaged over the entire frequency range are presented in Fig. 18 (bottom) and are largely independent of particle size (the 4- and 5-mm glass particles produce scattered results for the same reasons as in the group velocity). Consequently, the attenuation does not appear to scale with $1/\bar{D}$ as suggested by the dimensional arguments of Sec. IV. It seems clear that though the dynamics of the contact model give reasonable values for and scaling of the wave speeds (and therefore the normal stiffness seems correct), the attenuation and therefore the damping and perhaps the tangential components of the model are not adequate.

B. Constant-frequency experiments

Constant-frequency experiments provide some insight into the role that bed rearrangement has on wave propagation. The experiments were performed by first increasing the amplitude and then decreasing it. Figure 19 shows the effect of rearrangement by comparing an initially unconsolidated bed (in which relative particle motion is more likely) with a consolidated bed. In the unconsolidated case, the measured wave speed takes different values during the increase and decrease of the input acceleration level. Near the middle of the acceleration range, the difference is large, as much 100 m/s. This discrepancy is attributed to particle rearrangement in the granular bed. The act of passing pressure waves of increasing amplitude through the bed breaks and reforms the particle chains that serve as wave paths. In contrast, the consolidated case gives nearly the same speeds during increase and decrease. Further evidence of particle rearrangement can be seen in the scatter of the data. The scatter for the unconsolidated case is generally much larger than that for the consolidated case. Also, the scatter for the unconsolidated bed increases with piston acceleration amplitude. One would expect a larger force input at the piston to disturb more force chains and increase the variability of the data.

Despite these irregularities in the wave speed as the input acceleration is increased, some repeatability does exist at the largest amplitudes. Above accelerations of 0.3g, the wave speed in the unconsolidated bed takes a consistent value during both the increase and decrease of the piston amplitude. This suggests that, at large amplitudes, the waves themselves establish some uniformity in the state of the material near the piston.

Trends in the attenuation are similar, but more exaggerated, as seen in Fig. 19 (bottom). Again, rearrangement ap-

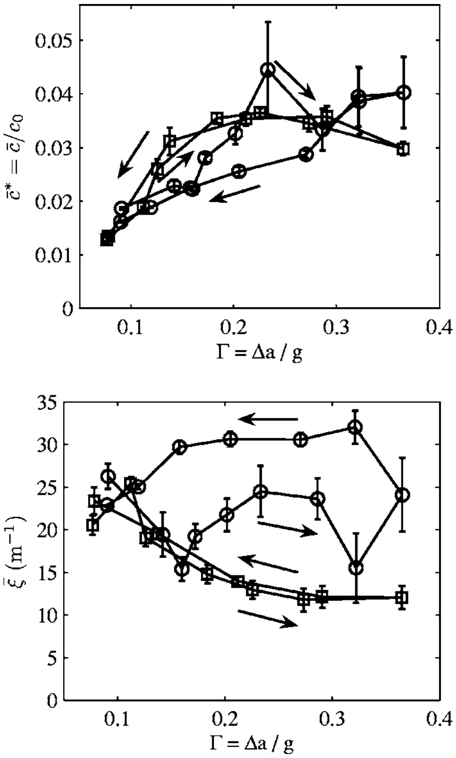

FIG. 19. Mean phase speed (top) and attenuation (bottom) for an unconsolidated bed (○) and a consolidated bed (□) as the acceleration amplitude of the input wave is increased and then decreased.

pears to lead to a lack of repeatability in the unconsolidated bed. Indeed, there is no consistency between measurements taken during amplitude increase and decrease at any value of the amplitude. A different mean value of the attenuation ratio is found over the entire range of accelerations. The scatter in the data is again suggestive of bed rearrangement. For the unconsolidated case, the scatter in the attenuation data increases slightly with acceleration. In contrast, the consolidated bed has less scatter and the scatter is roughly the same at all amplitudes.

VIII. SIMULATIONS WITH CONTINUOUS INPUT

Simulations were also carried out with continuous excitation. The pressures recorded at both walls were sinusoidal in shape, smooth, and relatively devoid of noise. To examine the wave propagation characteristics more closely, a series of frequencies was propagated into one particular bed configuration. The acceleration amplitude of the left wall was maintained constant (effectively applying a constant force amplitude to the bed), and the pressures at various locations were monitored. The phase shift between the pressure detected at the right wall and the displacement of the left wall was measured as a function of frequency. Straight line fits to those graphs lead to average dimensionless group velocities of 0.0525 and 0.048, respectively, at the lower and upper sensors. These values are in relatively good agreement with the experimental measurements [see Fig. 18 (top)]. They also exhibit the expected increase with depth in the bed.

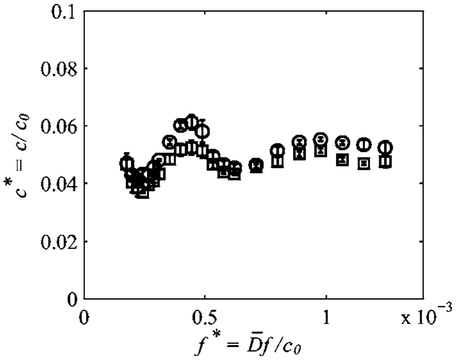

FIG. 20. Typical phase speeds calculated from the phase shift between the output pressure (right wall) and the displacement of the left wall. Measurements at 57 particle diameters (○) and 27 particle diameters (□) below the free surface.

Phase speeds were also calculated from that data and typical data is shown in Fig. 20. On average, the speed is roughly constant with frequency, confirming the nondispersive nature of wave propagation found in the experiments. As in the experiments there are some significant departures from the constant value. The departures are less scattered and more repeatable than in the experiments but they have no obvious explanation.

IX. SOME DETAILED ANALYSES

A. Nonlinear waves

The consequences of the nonlinearities inherent in the particle contact dynamics have been most systematically explored in the simpler context of one-dimensional (1D) particle chains. Nesterenko analyzed the propagation of waves in 1D chains and identified two different classes of solutions [21]. In one class defined by particle displacements that are small compared to the static overlap δ_0 (caused by a given mean compression force F_0) and termed a "strongly compressed chain," Nesterenko shows that nonlinear waves are governed by the Korteweg–de Vries equation [24,25] and the system therefore exhibits solitary waves and solitons. These have the characteristic that the width of the soliton increases with decreasing amplitude. The other, "weakly compressed" class is defined by particle displacements that are comparable to or larger than the initial overlap δ_0. Nesterenko shows that this leads to a different nonlinear wave equation but one that also exhibits solitary wave solutions. However, these solitons have the property that their width is independent of their amplitude; it is equal to about five particle diameters. Experiments on 1D chains have been carried out [26,27] and largely substantiate these theoretical results though the energy loss mechanisms limit the range of the measurements. The present paper indicates that these nonlinear phenomena may also occur in 3D granular beds.

The present simulations of pulse propagation in granular beds reveal pulse shapes (for example Fig. 12) whose shapes are quite consistent with those predicted by Nesterenko (see Ref. [14] for more details). The width of the "strongly compressed" pulses increases with decreasing amplitude as

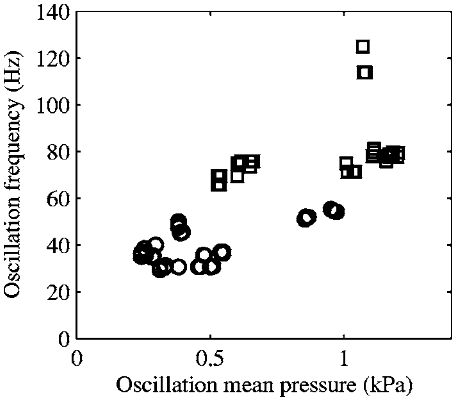

FIG. 21. Frequency of the oscillations after the passing of the initial peak plotted as a function of the mean pressure during the oscillations. Measurements were made in PVC (○) and 3-mm glass particles (□).

shown by comparing the primary and secondary peaks in Fig. 12. Moreover, at smaller widths we also observed a transition to waves whose width is independent of the amplitude. The discrepancy is that the granular bed produces a constant pulse width of the order of 100 particle diameters rather than the 5 diameters of the 1D chain. Perhaps the 100-particle-diameter dimension is related to the typical force chain length.

Despite the interesting similarities between the solitary waves of theory and the semipermanent waves observed in the present work, it is premature to draw a conclusive link between the two. The semipermanent waves were observed over short propagation distances due to high attenuation in the experiments and a limited size of the computational domain in the simulations. To determine whether the semipermanent waves are in fact solitary waves, they would need to be monitored over much greater propagation lengths.

B. Force chain ringing

We now shift our focus to the oscillations that are observed to follow the passage of a single pulse through a granular bed. Two different types of ringing were observed. Short-duration oscillations were seen at elevated pressures during [Fig. 5 (top), 41 ms and 65 ms widths] and just after [Fig. 5 (bottom), 6 ms width] the piston motion. These were characterized by a relatively smooth, sinusoidal shape and were limited to a maximum of three periods with various frequencies in the range 20–80 Hz. On the other hand, long-duration oscillations (lasting as long as 20 periods) were observed after the wave had passed. Their structure was comparatively noisy, but their frequency was consistently 20 Hz. The short-duration oscillation frequencies are plotted against the instantaneous mean pressure in Fig. 21. Note that this range of frequencies, 20–80 Hz, is much too low to be caused by natural vibrations of the transducer diaphragm or the piston system. One possible explanation is that they reflect a natural frequency of the force chains through which the waves travel.

In the force chain ringing scenario, one would expect the frequency to increase with the confining stress on the chain. Thus, ringing about an elevated pressure level should occur at a higher frequency than ringing about the static pressure. Though there is significant scatter in Fig. 21, there does appear to be an increase in the frequency with the mean pressure. Ringing about an elevated mean pressure consistently occurs at a higher frequency than that about lower pressures. This is consistent with the hypothesis that the oscillations are natural vibrations of the force chains.

To further discussion, we estimate the natural frequency of a force chain in a granular bed with Hertzian contacts (force given by $K_2\delta^{3/2}$) and an initial compression force F_0 that implies an initial particle overlap δ_0 between each pair of particles. The linearized stiffness at each contact will then be

$$k = \frac{dF}{d\delta} = \frac{3}{2}K_2\delta_0^{1/2}k = \frac{3}{2}K_2^{2/3}F_0^{1/3}. \tag{6}$$

Assuming that the force amplitudes associated with the pulses are much smaller than F_0 the natural frequency f_{nat} of the chain can be calculated as $f_{nat}=C\sqrt{k/m}$ where m is the mass of each particle and C is a factor that depends on the number of particles in the chain and the boundary conditions at the ends of the chain. In general, C decreases as the number of particles increases. For a chain of 100 particles with fixed ends, C is about 10^{-3}. For glass beads, $\sqrt{k/m}$ is about 10^5 Hz if the initial compression force is taken as the overburden of 8 cm. The result is a frequency on the order of 100 Hz which is in the range of the experimental observations (see Fig. 21).

X. DISCUSSION

In general, this paper reveals the depth of the complex issues associated with wave propagation in a granular bed. Experiments and simulations both show that there are various aspects to these complexities. First, and perhaps most readily understood, are the complexities introduced by the nonlinear response of the particle-particle contacts. These have been quite exhaustively explored by Nesterenko and others [28] in the context of one-dimensional particle chains where two classes of nonlinear waves can be identified, respectively for strongly and weakly compressed chains. We show that the experiments and simulations both indicate two similar regimes for wave propagation in a granular bed. There are, however, some quantitative differences. For example, the fixed solitary wave width for weakly compressed waves appears to be about 100 particle diameters in a granular bed compared with 5 particle diameters in a one-dimensional chain.

Another complexity is the ephemeral and fragile nature of the force chains along which the pressure waves in a granular bed are primarily transmitted. As previously identified by Liu and Nagel (see also Jia *et al.*), this leads to considerable difficulty in acquiring repeatable data on wave propagation speeds and attenuation. In this paper the transmission of single pulses and of continuous sinusoidal waves has been explored both experimentally and through simulations.

The continuous excitation investigations confirm the conclusion of Liu and Nagel that waves below a critical frequency (identified by Jia *et al.*) are nearly nondispersive; however, there are some minor variations in the wave speed with frequency that are most apparent and repeatable in the simulations and could be responsible for some weak dispersion. However, the attenuation is sufficiently strong that such long-term effects cannot be observed in the experiments. We also note that, like the wave propagation speeds, the attenuation data exhibit considerable scatter. However, the measurements are sufficiently accurate to confirm the results of a dimensional analysis which shows that the wave speed is primarily a function of the wave speed in the material of the particles, Poisson's ratio for that material, and the geometric arrangement of the particles; it is not a function of particle size. Nondimensional analysis also suggests that the attenuation should be inversely proportional to particle size. Such a dependence is not observed in the experiments, such that further consideration needs to be given to the damping and tangential friction components of the contact model.

Both the scatter in the measurements and the hysteretic effects during frequency and amplitude sweeps were greater in unconsolidated beds than in consolidated beds in which particle mobility is reduced. The scatter is also greater for larger ratios of particle size to transducer size since the measurement then records an average over very few force chains. This evidence is consistent with that of Liu and Nagel and supports the conjecture that there is continual rearrangement of the particles and particle chains as a result of the waves themselves.

The experiments and simulations utilizing single input pulses revealed further aspects of wave propagation in granular beds. Though the pulses were rapidly attenuated with distance (exponential decay at a greater rate in the plastic than in the glass), it was nevertheless possible to identify several basic phenomena. First, increasing disruption of the force chains was observed as the pulse amplitude increased (either by increasing the input pulse or by observing the consequences at different penetrations into the granular bed). Second, as mentioned above, the nonlinearity in the contact point dynamics leads to two regimes of nonlinear waves just as was predicted and observed in one-dimensional particle chains by Nesterenko and others. Short input pulses lead to transmitted pulses with a fixed width of about 100 particle diameters (compared to the 5 particle diameters in one-dimensional chains). Long input pulses lead to transmitted waves consisting of a lead pulse and a train of trailing waves. One conjecture which we put forward here is that these trailing waves whose frequency is in the range 20–80 Hz (increasing systematically with prevailing pressure) are caused by a ringing of the force chains.

The simulations of the pulse propagation reveal further details, such as the increasing distortion of the wave front as the pulse progresses through the granular material and specific dependences of the wave propagation on other material properties such as Poisson's ratio (for details see Ref. [14]).

---

[1] W. Gregor and H. Rumpf, Int. J. Multiphase Flow **1**, 753 (1975).
[2] D. Musmarra, M. Poletto, S. Vaccaro, and R. Clift, Powder Technol. **82**, 255 (1995).
[3] G. J. Weir, Chem. Eng. Sci. **56**, 3699 (2001).
[4] G. Ben-Dor, A. Britan, T. Elperin, O. Igra, and J. Jiang, Exp. Fluids **22**, 432 (1997).
[5] B. Hardin and F. Richart, J. Soil Mech. Found. Div. **89**, 33 (1963).
[6] J. Duffy and R. Mindlin, J. Appl. Mech. **24**, 585 (1957).
[7] W. Goldsmith, *Impact* (Edward Arnold, London, 1960).
[8] K. Johnson, *Contact Mechanics* (Cambridge University Press, Combridge, England, 1987).
[9] J. Goddard, Proc. R. Soc. London, Ser. A **430**, 105 (1990).
[10] H. A. Makse, N. Gland, D. L. Johnson, and L. M. Schwartz, Phys. Rev. Lett. **83**, 5070 (1999).
[11] B. Velický and C. Caroli, Phys. Rev. E **65**, 021307 (2002).
[12] C. H. Liu and S. R. Nagel, Phys. Rev. Lett. **68**, 2301 (1992).
[13] X. Jia, C. Caroli, and B. Velicky, Phys. Rev. Lett. **82**, 1863 (1999).
[14] S. R. Hostler, Ph.D. thesis, California Institute of Technology, 2005.
[15] P. Cundall and O. Strack, Geotechnique **29**, 47 (1979).
[16] J. Geng, D. Howell, E. Longhi, R. Behringer, G. Reydellet, L. Vanel, E. Clément, and S. Luding, Phys. Rev. Lett. **87**, 035506 (2001).
[17] C. Liu and S. R. Nagel, Phys. Rev. B **48**, 15646 (1993).
[18] C. S. Campbell and C. E. Brennen, J. Fluid Mech. **151**, 167 (1985).
[19] N. V. Brilliantov, F. Spahn, J.-M. Hertzsch, and T. Pöschel, Phys. Rev. E **53**, 5382 (1996).
[20] C. R. Wassgren, Ph.D. thesis, California Institute of Technology, 1997.
[21] V. F. Nesterenko, *Dynamics of Heterogeneous Materials* (Springer-Verlag, New York, 2001).
[22] J. R. Zenit, Ph.D. thesis, California Institute of Technology, 1997.
[23] C. Liu and S. R. Nagel, J. Phys.: Condens. Matter **6**, A433 (1994).
[24] G. B. Whitham, *Linear and Nonlinear Waves* (Wiley, New York, 1974).
[25] S. Leibovich and A. R. Seebass, *Nonlinear Waves* (Cornell University Press, Ithaca, NY, 1978).
[26] A. Lazaridi and V. Nesterenko, J. Appl. Mech. Tech. Phys. **26**, 45 (1985).
[27] C. Coste, E. Falcon, and S. Fauve, Phys. Rev. E **56**, 6104 (1997).
[28] S. Sen, M. Manciu, R. S. Sinkovits, and A. J. Hurd, Granular Matter **3**, 33 (2001).